Omnidirectional reflection from generalized Fibonacci quasicrystals

Alberto G. Barriuso,[1] Juan J. Monzón,[1] Teresa Yonte,[1], Angel Felipe[2], and Luis L. Sánchez-Soto[1*]

[1]*Departamento de Óptica, Universidad Complutense, 28040 Madrid, Spain*
[2]*Departamento de Estadística e Investigación Operativa I, Facultad de Matemáticas, Universidad Complutense, 28040 Madrid, Spain*

[*]*lsanchez@fis.ucm.es*

Abstract: We determine the optimal thicknesses for which omnidirectional reflection from generalized Fibonacci quasicrystals occurs. By capitalizing on the idea of wavelength- and angle-averaged reflectance, we assess in a consistent way the performance of the different systems. Our results indicate that some of these aperiodic arrangements can largely overperform the conventional photonic crystals as omnidirectional reflection is concerned.

OCIS codes: (160.5293) Photonic bandgap materials; (230.5298) Photonic crystals; (310.4165) Multilayer design; (350.4238) Nanophotonics and photonic crystals.

References and links

1. J. D. Joannopoulos, R. D. Meade, J. N. Winn, and R. D. Meade, *Photonic Crystals: Molding the Flow of Light*, 2nd ed. (Princeton University, 2008).
2. K. Busch, G. von Freymann, S. Linden, S. Mingaleev, L.Tkeshelashvili, and M. Wegenerd, "Periodic nanostructures for photonics," Phys. Rep. **444**, 101–202 (2007).
3. B. Kramer and A. MacKinnon, "Localization: Theory and experiment," Rep. Prog. Phys. **56**, 1469–1564 (1993).
4. M. Segev, Y. Silberberg, and D. N. Christodoulides, "Anderson localization of light," Nat. Photonics **7**, 197–204 (2013).
5. A. Lagendijk and B. A. van Tiggelen, "Resonant multiple scattering of light," Phys. Rep. **270**, 143–215 (1996).
6. B. A. van Tiggelen, "Transverse diffusion of light in Faraday-active media," Phys. Rev. Lett. **75**, 422–424 (1995).
7. W. Steurer and D. Sutter-Widmer, "Photonic and phononic quasicrystals," J. Phys. D **40**, R229–R247 (2007).
8. A. Poddubny and E. Ivchenko, "Photonic quasicrystalline and aperiodic structures," Physica E **42**, 1871–1895 (2010).
9. L. Dal Negro and S. V. Boriskina, "Deterministic aperiodic nanostructures for photonics and plasmonics applications," Laser Photon. Rev. **6**, 178–218 (2012).
10. P. J. Steinhardt and S. Ostlund, *The Physics of Quasicrystals* (World Scientific, 1987).
11. M. Senechal, *Quasicrystals and Geometry* (Cambridge University, 1995).
12. C. Janot, *Quasicrystals: A Primer* (Oxford University, 2012).
13. Z. V. Vardeny, A. Nahata, and A. Agrawal, "Optics of photonic quasicrystals," Nat. Photonics **7**, 177–187 (2013).
14. E. Maciá, "The role of aperiodic order in science and technology," Rep. Prog. Phys. **69**, 397–441 (2006).
15. E. Maciá, *Aperiodic Structures in Condensed Matter: Fundamentals and Applications* (CRC, 2009).
16. R. Merlin, K. Bajema, R. Clarke, F. Y. Juang, and P. K. Bhattacharya, "Quasiperiodic GaAs-AlAs heterostructures," Phys. Rev. Lett. **55**, 1768–1770 (1985).
17. M. Kohmoto, L. P. Kadanoff, and C. Tang, "Localization problem in one dimension: Mapping and escape," Phys. Rev. Lett. **50**, 1870–1872 (1983).
18. M. Kohmoto, B. Sutherland, and K. Iguchi, "Localization in optics: Quasiperiodic media," Phys. Rev. Lett. **58**, 2436–2438 (1987).
19. N.-H. Liu, "Propagation of light waves in Thue-Morse dielectric multilayers," Phys. Rev. B **55**, 3543–3547 (1997).
20. S. Tamura and F. Nori, "Transmission and frequency spectra of acoustic phonons in Thue-Morse superlattices," Phys. Rev. B **40**, 9790–9801 (1989).

#198470 - $15.00 USD Received 1 Oct 2013; revised 14 Nov 2013; accepted 15 Nov 2013; published 27 Nov 2013

21. M. Kolář, M. K. Ali, and F. Nori, "Generalized Thue-Morse chains and their physical properties," Phys. Rev. B **43**, 1034–1047 (1991).
22. J. M. Luck, "Cantor spectra and scaling of gap widths in deterministic aperiodic systems," Phys. Rev. B **39**, 5834–5849 (1989).
23. C. Sibilia, I. S. Nefedov, M. Scalora, and M. Bertolotti, "Electromagnetic mode density for finite quasi-periodic structures," J. Opt. Soc. Am. B **15**, 1947–1952 (1998).
24. E. Cojocaru, "Forbidden gaps in finite periodic and quasi-periodic Cantor-like dielectric multilayers at normal incidence," Appl. Opt. **40**, 6319–6326 (2001).
25. A. V. Lavrinenko, S. V. Zhukovsky, K. S. Sandomirski, and S. V. Gaponenko, "Propagation of classical waves in nonperiodic media: Scaling properties of an optical cantor filter," Phys. Rev. E **65**, 036621 (2002).
26. S. V. Zhukovsky, A. V. Lavrinenko, and S. V. Gaponenko, "Spectral scalability as a result of geometrical self-similarity in fractal multilayers," Europhys. Lett. **66**, 455–461 (2004).
27. G. Gumbs and M. K. Ali, "Dynamical maps, Cantor spectra, and localization for Fibonacci and related quasiperiodic lattices," Phys. Rev. Lett. **60**, 1081–1084 (1988).
28. F. Nori and J. P. Rodríguez, "Acoustic and electronic properties of one-dimensional quasicrystals," Phys. Rev. B **34**, 2207–2211 (1986).
29. E. Maciá and F. Domínguez-Adame, "Physical nature of critical wave functions in Fibonacci systems," Phys. Rev. Lett. **76**, 2957–2960 (1996).
30. T. Fujiwara, M. Kohmoto, and T. Tokihiro, "Multifractal wave functions on a Fibonacci lattice," Phys. Rev. B **40**, 7413–7416 (1989).
31. J. A. Monsoriu, F. R. Villatoro, M. J. Marín, J. Pérez, and L. Monreal, "Quantum fractal superlattices," Am. J. Phys. **74**, 831–836 (2006).
32. P. Yeh, *Optical Waves in Layered Media* (Wiley, 1988).
33. J. Lekner, *Theory of Reflection* (Kluwer, 1987).
34. Y. Fink, J. N. Winn, S. Fan, C. Chen, J. Michel, J. D. Joannopoulos, and E. L. Thomas, "A dielectric omnidirectional reflector," Science **282**, 1679–1682 (1998).
35. J. P. Dowling, "Mirror on the wall: you're omnidirectional after all?" Science **282**, 1841–1842 (1998).
36. E. Yablonovitch, "Engineered omnidirectional external-reflectivity spectra from one-dimensional layered interference filters," Opt. Lett. **23**, 1648–1649 (1998).
37. D. N. Chigrin, A. V. Lavrinenko, D. A. Yarotsky, and S. V. Gaponenko, "All-dielectric one-dimensional periodic structures for total omnidirectional reflection and partial spontaneous emission control," J. Lightw. Technol. **17**, 2018–2024 (1999).
38. D. N. Chigrin, A. V. Lavrinenko, D. A. Yarotsky, and S. V. Gaponenko, "Observation of total omnidirectional reflection from a one-dimensional dielectric lattice," Appl. Phys. A **68**, 25–28 (1999).
39. J. Lekner, "Omnidirectional reflection by multilayer dielectric mirrors," J. Opt. A **2**, 349–352 (2000).
40. D. Lusk, I. Abdulhalim, and F. Placido, "Omnidirectional reflection from Fibonacci quasi-periodic one-dimensional photonic crystal," Opt. Commun. **198**, 273–279 (2001).
41. F. Qiu, R. W. Peng, X. Q. Huang, X. F. Hu, M. Wang, A. Hu, S. S. Jiang, and D. Feng, "Omnidirectional reflection of electromagnetic waves on Thue-Morse dielectric multilayers," Europhys. Lett. **68**, 658–663 (2004).
42. T. Yonte, J. J. Monzón, A. Felipe, and L. L. Sánchez-Soto, "Optimizing omnidirectional reflection by multilayer mirrors," J. Opt. A **6**, 127–131 (2004).
43. A. G. Barriuso, J. J. Monzón, L. L. Sánchez-Soto, and A. Felipe, "Integral merit function for broadband omnidirectional mirrors," Appl. Opt. **46**, 2903–2906 (2007).
44. A. G. Barriuso, J. J. Monzón, L. L. Sánchez-Soto, and A. Felipe, "Comparing omnidirectional reflection from periodic and quasiperiodic one-dimensional photonic crystals," Opt. Express **13**, 3913–3920 (2005).
45. M. Holzer, "Three classes of one-dimensional, two-tile Penrose tilings and the Fibonacci Kronig-Penney model as a generic case," Phys. Rev. B **38**, 1709–1720 (1988).
46. M. Severin, M. Dulea, and R. Riklund, "Periodic and quasiperiodic wavefunctions in a class of one-dimensional quasicrystals: an analytical treatment," J. Phys.: Condens. Matter **1**, 8851–8858 (1989).
47. M. Dulea, M. Severin, and R. Riklund, "Transmission of light through deterministic aperiodic non-Fibonaccian multilayers," Phys. Rev. B **42**, 3680–3689 (1990).
48. A. Chakrabarti and S. N. Karmakar, "Renormalization-group method for exact Green's functions of self-similar lattices: Application to generalized Fibonacci chains," Phys. Rev. B **44**, 896–899 (1991).
49. X. Fu, Y. Liu, P. Zhou, and W. Sritrakool, "Perfect self-similarity of energy spectra and gap-labeling properties in one-dimensional Fibonacci-class quasilattices," Phys. Rev. B **55**, 2882–2889 (1997).
50. X. Wang, U. Grimm, and M. Schreiber, "Trace and antitrace maps for aperiodic sequences: Extensions and applications," Phys. Rev. B **62**, 14020–14031 (2000).
51. Y. Chen, X. Yang, Q. Guo, and S. Lan, "Second-harmonic generation in GF(m, 1) ferroelectric superlattices," J. Phys.: Condens. Matter **18**, 2587–2600 (2006).
52. S. Thiem, M. Schreiber, and U. Grimm, "Wave packet dynamics, ergodicity, and localization in quasiperiodic chains," Phys. Rev. B **80**, 214203 (2009).
53. S. Thiem and M. Schreiber, "Photonic properties of metallic-mean quasiperiodic chains," Eur. Phys. J. B **76**,

#198470 - $15.00 USD Received 1 Oct 2013; revised 14 Nov 2013; accepted 15 Nov 2013; published 27 Nov 2013

339–345 (2010).
54. Z. Zhang, P. Tong, J. Gong, and B. Li, "Wave packet dynamics in one-dimensional linear and nonlinear generalized Fibonacci lattices," Phys. Rev. E **83**, 056205 (2011).
55. S. Thiem, M. Schreiber, and U. Grimm, "Light transmission through metallic-mean quasiperiodic stacks with oblique incidence," Philos. Mag. **91**, 2801–2810 (2011).
56. C. H. O. Costa and M. S. Vasconcelos, "Band gaps and transmission spectra in generalized Fibonacci $\sigma(p,q)$ one-dimensional magnonic quasicrystals," J. Phys.: Condens. Matter **25**, 286002 (2013).
57. V. W. Spinadel, "The metallic means family and multifractal spectra," Nonlinear Anal. **36**, 721–745 (1999).
58. M. Lothaire, *Combinatorics on Words*, 2nd ed. (Cambridge University, 1997).
59. M. Queffélec, *Substitutional Dynamics Systems – Spectral Analysis* (Springer, 1987).
60. R. A. Dunlap, *The Golden Ratio and Fibonacci Numbers* (World Scientific, 1997).
61. E. Bombieri and J. E. Taylor, "Which distributions of matter diffract? an initial investigation," J. Phys. Colloq. **47**, 19–28 (1986).
62. E. Bombieri and J. Taylor, "Quasicrystals, tilings, and algebraic number theory," Contemp. Math. **64**, 241–264 (1987).
63. C. Godrèche and J. M. Luck, "Indexing the diffraction spectrum of a non-Pisot self-similar structure," Phys. Rev. B **45**, 176–185 (1992).
64. C. D. Meyer, *Matrix Analysis and Applied Linear Algebra* (Society for Industrial and Applied Mathematics, 2000).
65. M. Severin and R. Riklund, "Using the Fourier spectrum to classify families of generalised extensions of the Fibonaccian lattice," J. Phys.: Condens. Matter **1**, 5607–5612 (1989).
66. Z. Cheng and R. Savit, "Structure factor of substitutional sequences," J. Stat. Phys. **60**, 383–393 (1990).
67. J. Bellissard, A. Bovier, and J. M. Ghez, "Gap labelling theorems for one-dimensional discrete Schrödinger operators," Rev. Math. Phys. **4**, 1–37 (1992).
68. M. Dulea, M. Johansson, and R. Riklund, "Localization of electrons and electromagnetic waves in a deterministic aperiodic system," Phys. Rev. B **45**, 105–114 (1992).
69. G. Y. Oh and M. H. Lee, "Band-structural and Fourier-spectral properties of one-dimensional generalized Fibonacci lattices," Phys. Rev. B **48**, 12465–12477 (1993).
70. L. L. Sánchez-Soto, J. J. Monzón, A. G. Barriuso, and J. F. Cariñena, "The transfer matrix: A geometrical perspective," Phys. Rep. **513**, 191–227 (2012).
71. J. F. Tang and Q. Zheng, "Automatic design of optical thin-film systems: merit function and numerical optimization method," J. Opt. Soc. Am. **72**, 1522–1528 (1982).
72. J. A. Dobrowolski, F. C. Ho, A. Belkind, and V. A. Koss, "Merit functions for more effective thin film calculations," Appl. Opt. **28**, 2824–2831 (1989).
73. A. Premoli and M. L. Rastello, "Minimax refining of wideband antireflection coatings for wide angular incidence," Appl. Opt. **33**, 2018–2024 (1994).
74. D. T. F. Marple, "Refractive index of ZnSe, ZnTe, and CdTe," J. Appl. Phys. **35**, 539–542 (1964).
Southwell:1999vn
75. W. H. Southwell, "Omnidirectional mirror design with quarter-wave dielectric stacks," Appl. Opt. **38**, 5464–5467 (1999).
76. S. V. Zhukovsky and S. V. Gaponenko, "Constraints on transmission, dispersion, and density of states in dielectric multilayers and stepwise potential barriers with an arbitrary layer arrangement," Phys. Rev. E **77**, 046602 (2008).
77. V. Grigoriev and F. Biancalana, "Exact analytical representations for broadband transmission properties of quarter-wave multilayers," Opt. Lett. **36**, 3774–3776 (2011).

1. Introduction

The spatial modulation of the dielectric properties of a medium brings about substantial modifications in light propagation. When the spatial profile is periodic, the resulting structure is called a photonic crystal, underlining the strong similarities between the distinctive features of light in these structures and those of electrons in semiconductors [1, 2].

The converse case of a random spatial distribution has also attracted a lot of attention, for it is at the root of a good many effects, such as Anderson localization [3, 4], coherent backscattering [5], and optical Hall effect [6], to cite only a few.

Deterministic and yet nonperiodic spatial patterns, dubbed photonic quasicrystals [7–13], fill the heap of room in between the two aforementioned extreme examples. Even if propagation in these intriguing arrangements is not thoroughly understood, it has been recently recognized that they can provide remarkable functionalities [14, 15]. This is of utmost significance, because the rich variety of aperiodic structures adds considerable versatility when engineering the optical

#198470 - $15.00 USD Received 1 Oct 2013; revised 14 Nov 2013; accepted 15 Nov 2013; published 27 Nov 2013

response of feasible devices.

The first illustration of an aperiodic lattice possessing long-range order was a one-dimensional semiconductor heterostructure assembled according to the Fibonacci sequence [16–18]. Subsequently, a wealth of photonic quasicrystals have been conceived, the most outstanding ones being Thue-Morse [19–21] and Cantor [22–26]. Both classical (light) and quantum (electrons) waves in these media have been shown to have a self-similar energy spectrum [27], a pseudo-bandgap of forbidden frequencies [28], and critically localized states [29] whose wave functions are distinguished by power law asymptotes and self-similarity [30, 31].

Bragg mirrors, consisting of alternating low- and high-index layers, constitute the simplest example of one-dimensional photonic crystals [32, 33]. In particular, quarter-wave stacks are the most extensively studied in connection with omnidirectional reflection (ODR); that is, they present ranges of frequency in which strong reflection occurs for all angles of incidence and all polarizations [34–39].

The possibility of achieving ODR from Fibonacci [40] and Thue-Morse [41] quasicrystals has been put forward lately. However, in those analysis ODR is treated in the limit of an infinite span. In practice, every system is finite and one needs to quantify ODR in a manner that permits unambiguous comparison between different layouts. An appropriate tool for that end is the wavelength- and angle-averaged reflectance [42, 43]. Putting this concept to work is relatively straightforward and one is right away led to the conclusion that, for the same number of layers, photonic crystals always offer better performance than Fibonacci or Thue-Morse ones [44].

This upshot seems to rule out any potential benefit of quasicrystals as ODRs. In spite of this, we examine in this work the so-called generalized Fibonacci quasicrystals. This notion has developed into a rich field of research [45–56], which besides is buttressed by a list of remarkable mathematical properties [57], to the extent that there is a journal entirely devoted to this stuff; the Fibonacci Quarterly.

Surprisingly, the ODR properties of the generalized Fibonacci quasicrystals have not yet been explored; such is precisely the goal of this paper. Indeed, we find out that these schemes can exhibit superior ODR performance than the photonic crystals. Only in the narrowband approximation, the latter maintain their supremacy. This unforeseen result opens new perspectives for generalized quasicrystals and confirms once again that interference works in mysterious ways.

The plan of this paper is as follows. In Sec. 2 we provide a brief account of the mathematical concepts involved in these generalized quasycristals. Expedient methods to determine their optical response are outlined in Sec. 3. With all this machinery at hand, we proceed to scrutinize the ODR performance: in Sec. 4, we restrict ourselves to the narrowband limit, whereas the general broadband case is considered in Sec. 5. Finally, our conclusions are summarized in Sec. 6.

2. Generalized Fibonacci sequences

A sequence (also called a word) is an ordered list made up of letters, which are elements of a finite alphabet. We shall be mainly engaged in a two-letter alphabet, denoted by $\{L,H\}$, but alphabets can be of any size. In physical realizations, each letter corresponds to a different type of building block (e.g., dielectric layers, nanoparticles, etc).

A time-honored method to generate deterministic aperiodic sequences relies on symbolic substitutions [58, 59]. A specific substitution rule replaces each letter in the alphabet by a finite word, viz

$$L \mapsto \varphi_1(L,H)\,, \qquad H \mapsto \varphi_2(L,H)\,, \tag{1}$$

where φ_1 and φ_2 can be any string of L and H. In addition, one must start from a given letter, which is called a seed or initiator.

#198470 - $15.00 USD Received 1 Oct 2013; revised 14 Nov 2013; accepted 15 Nov 2013; published 27 Nov 2013

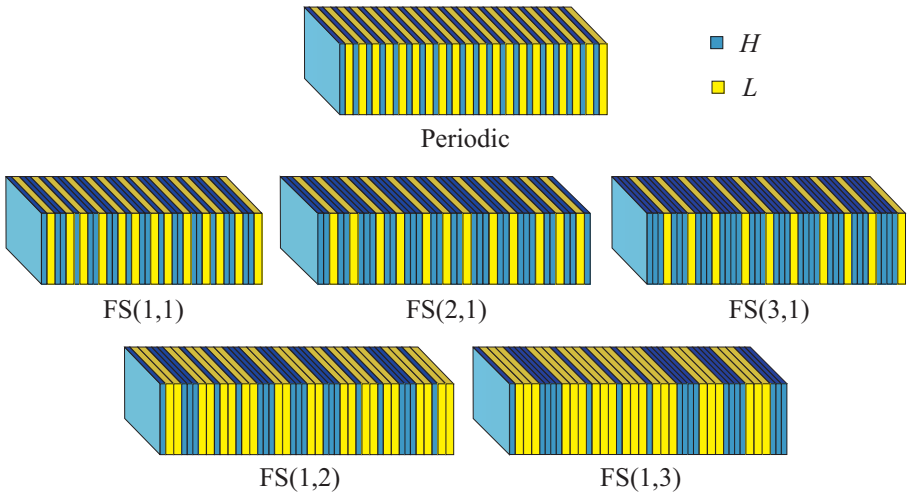

Fig. 1. Illustrating different arrangements considered in this work. In the top panel, we have the periodic case (40 letters). In the mid panel, the Olympic-metal family FS (h,1), with (from left to right) $h = 1$ (golden mean, 34 letters), $h = 2$ (silver mean, 41 letters), and $h = 3$ (bronze mean, 43 letters). In the bottom panel, the non-Olympic-metal family FS (1, ℓ), with $\ell = 2$ (copper mean, 43 letters) and $\ell = 3$ (nickel mean, 40 letters). The differences can be appreciated at a simple glance.

More concretely, we are interested in the generalized Fibonacci sequences FS(h,ℓ), which are generated by the inflation rule

$$L \mapsto H\,, \qquad\qquad H \mapsto H^h L^\ell\,, \tag{2}$$

where ℓ and h are arbitrary positive integers and we adopt the convention that the seed is L. Alternatively, the words $\{W_\alpha\}$ of FS(h,ℓ) are defined through the scheme

$$W_{\alpha+1} = W_\alpha^h W_{\alpha-1}^\ell\,, \tag{3}$$

with $W_0 = L$ and $W_1 = H$. Here the integer α labels the corresponding iteration, which is also known as the generation.

The length (i.e., the total number of letters L and H) of the word W_α is denoted by w_α and satisfies the recursion relation

$$w_{\alpha+1} = h\,w_\alpha + \ell w_{\alpha-1}\,. \tag{4}$$

In the limit of an infinite sequence, the lengths of two successive words satisfy

$$\lim_{\alpha\to\infty} \frac{w_\alpha}{w_{\alpha-1}} \equiv \sigma(h,\ell) = \frac{1}{2}(h + \sqrt{h^2+4\ell})\,. \tag{5}$$

For $\ell = 1$, the resulting sequence fulfills

$$\sigma(h,1) = [\bar{h}]\,, \tag{6}$$

$[\bar{h}]$ being the irrational number with a continued-fraction representation $[\bar{h}] = [h,h,h,\ldots]$ [57]. In particular, for $h = 1$ (the standard Fibonacci sequence) we get the golden mean, $\sigma(1,1) = \Phi = (1+\sqrt{5})/2$, for $h = 2$ the silver mean, $\sigma(2,1) = 1+\sqrt{2}$, for $h = 3$ the bronze mean $\sigma(3,1) = (3+\sqrt{13})/2$, and so on. This family generalizes in quite a natural way the golden ratio [60] and will be designated here, by obvious reasons, the Olympic-metal family.

#198470 - $15.00 USD Received 1 Oct 2013; revised 14 Nov 2013; accepted 15 Nov 2013; published 27 Nov 2013

On the other hand, when we fix $h = 1$, the sequences are, for instance,

$$\sigma(1,2) = [2,\overline{0}], \qquad \sigma(1,3) = [2,\overline{3}], \tag{7}$$

and the like. These two examples are known as the copper and nickel means and the complete FS(1, h) series will be termed as the non-Olympic-metal family. In Fig. 1 we roughly schematize some of these strings.

To each substitution rule (1) we associate a substitution matrix T, defined as

$$\mathsf{T} = \begin{pmatrix} |\varphi_1(L,H)|_L & |\varphi_2(L,H)|_L \\ |\varphi_1(L,H)|_H & |\varphi_2(L,H)|_H \end{pmatrix}, \tag{8}$$

where $|\cdot|_{L,H}$ is the number of letters L (resp. H). This matrix does not depend on the precise form of the substitutions, only on the number of letters L or H. The eigenvalues of T contain a lot of information. Actually, as discovered by Bombieri and Taylor [61, 62], if the spectrum of T contains a Pisot number as an eigenvalue, the sequence is quasiperiodic; otherwise it is not (and then is purely aperiodic). We recall that a Pisot number is a positive algebraic number (i.e., a number that is a solution of an algebraic equation) greater than one, all of whose conjugate elements (the other solutions of the defining algebraic equation) have modulus less than unity [63].

For FS(h,ℓ) we have

$$\mathsf{T}_{h,\ell} = \begin{pmatrix} h & 1 \\ \ell & 0 \end{pmatrix}, \tag{9}$$

whose eigenvalues are

$$\tau_{h,\ell}^{(\pm)} = \frac{1}{2}\left(h \pm \sqrt{h^2+4\ell}\right). \tag{10}$$

Incidentally, the largest eigenvalue $\tau_{h,\ell}^{(+)}$, which is often known as the Perron-Frobenius eigenvalue [64], coincides with the ratio $\sigma(h,\ell)$.

The eigenvalues $\tau_{h,1}$ are Pisot numbers, so all the sequences in the Olympic-metal family FS$(h,1)$ are quasiperiodic. In contradistinction, $\tau_{1,\ell}$ are not Pisot numbers and the corresponding non-Olympic-metal systems FS $(1,\ell)$, are aperiodic.

The main differences of these two situations can be appreciated by the nature of their Fourier spectrum [65]. For a specific word of length N, the discrete Fourier transform reads

$$\hat{W}_N(k) = \frac{1}{\sqrt{N}} \sum_{j=1}^{N-1} W(j) \exp\left(\frac{-2\pi i jk}{N}\right), \qquad k = 1,2\ldots,N, \tag{11}$$

where $W(j)$ is a numerical array obtained from the word by assigning to each letter of the alphabet a fixed number. This assignment is otherwise arbitrary and does not change any conclusion. In consequence, one could, e.g., use $L \mapsto -1$ and $H \mapsto 1$. The structure factor (or power spectrum) is [66]

$$F_N(k) = |\hat{W}_N(k)|^2. \tag{12}$$

From a rigorous perspective, the only well-established concept attached to the Fourier spectrum is its spectral measure. If $d\nu_N(k) = F_N(k)\,dk$, we will be concerned with the nature of the limit $d\nu(k) = \lim_{N\to\infty} d\nu_N(k)$, which corresponds to an infinite structure and a continuous variable k. Just as any positive measure, $d\nu(k)$ has a unique decomposition

$$d\nu(k) = d\nu_{\rm pp}(k) + d\nu_{\rm ac}(k) + d\nu_{\rm sc}(k) \tag{13}$$

#198470 - $15.00 USD Received 1 Oct 2013; revised 14 Nov 2013; accepted 15 Nov 2013; published 27 Nov 2013

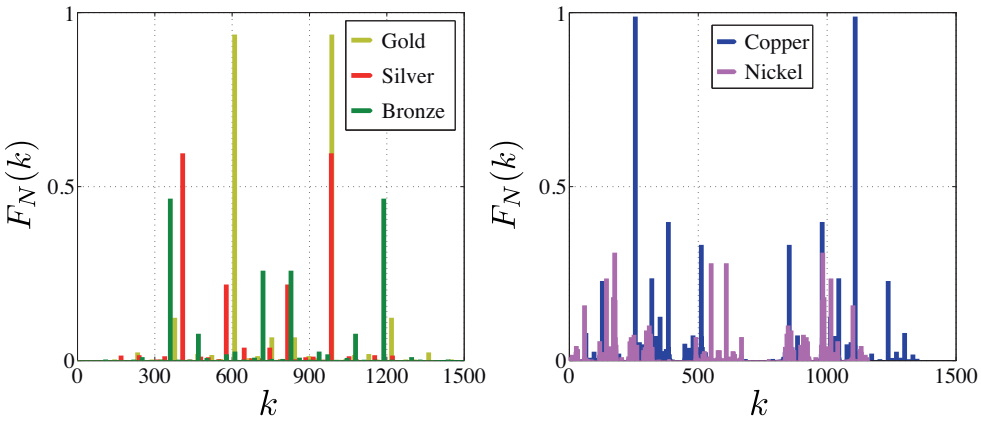

Fig. 2. Normalized power spectrum for words up to 1500 letters for different generalized Fibonacci sequences. In the left panel, for the Olympic-metal family FS(h,1), with $h = 1, 2,$ and 3. In the right panel, for the non-Olympic-metal sequences FS(1,2) and FS(1,3).

into its pure point, absolutely continuous and singular continuous parts [15]. The pure point part refers to the presence of Bragg peaks; the absolute continuous part is a differentiable function (diffuse scattering), while the singular continuous part it is neither continuous nor does it have Bragg peaks; it shows broad peaks, which are never isolated and, with increasing resolution, split again into further broad.

In Fig. 2 we have plotted the power spectrum $F_N(k)$ for the Olympic- and non-Olympic-metal families. The former, exhibit δ-like Bragg peaks that can be properly labeled in terms of the eigenvalues $\tau_{h,1}$ as

$$k_{m_1 m_2} = \frac{2\pi}{\Lambda_0} m_1 \tau_{h,1}^{m_2}, \tag{14}$$

with m_1 and m_2 integers and Λ_0 being a suitable average period of the structure. We can verify the existence of incommensurate intervals between peaks, confirming the quasiperiodicity of these arrangements. Moreover, a relevant result, known as the gap-labelling theorem [67, 68], relates the position of the peaks in Eq. (14) with the location of the gaps in the energy spectra of the elementary excitations supported by the structure.

For non-Olympic metals, the global structure looks blurred. Individual Bragg peaks are not separated by well-defined intervals, but tend to cluster forming “broad bands”. The strength of the dominant peaks is considerably bigger for the copper, which suggests that the nickel-mean lattice is more disordered than the copper one. A complete account of these issues is outside the scope of this work; however, a thorough analysis [69] shows that these spectra are multifractal and their Fourier-spectral measures are singular continuous ones.

3. Optical response

In an optical implementation of the generalized Fibonacci sequences FS (h, ℓ), the letters in the alphabet $\{L, H\}$ are realized as layers made of materials with refractive indices (n_L, n_H) and thicknesses (d_L, d_H), respectively. The material L has a low refractive index, while H is of a high refractive index, which justifies the notation employed thus far.

To properly compare the optical response we take advantage of the transfer-matrix tech-

#198470 - $15.00 USD Received 1 Oct 2013; revised 14 Nov 2013; accepted 15 Nov 2013; published 27 Nov 2013

nique [70]. For a single layer, say L, the transfer matrix reads as

$$\mathsf{M}_L(\theta,\lambda) = \begin{pmatrix} \cos\beta_L & -q_L \sin\beta_L \\ \dfrac{1}{q_L}\sin\beta_L & \cos\beta_L \end{pmatrix}. \tag{15}$$

Here, $\beta_L = (2\pi/\lambda) n_L d_L \cos\theta_L$ is the layer phase thickness, θ_L being the angle of refraction, which is determined by Snell's law. The wavelength in vacuum of the incident radiation is λ. The parameter q_L can be written for each basic polarization (parallel $\parallel$ or perpendicular $\perp$) as

$$q_L^{\parallel} = \frac{n_L \cos\theta}{\cos\theta_L}, \qquad q_L^{\perp} = \frac{\cos\theta}{n_L \cos\theta_L}. \tag{16}$$

For simplicity, we have assumed that the layer is imbedded in air and henceforth θ will indicate the incidence angle. Expressions completely analogous hold for the layer H.

According to Eq. (3), the αth word of FS(h,ℓ) has the associated transfer matrix

$$\mathsf{M}_{\alpha+1} = \mathsf{M}_{\alpha}^{h}\, \mathsf{M}_{\alpha-1}^{\ell}, \tag{17}$$

starting from $\mathsf{M}_0 = \mathsf{M}_L$ and $\mathsf{M}_1 = \mathsf{M}_H$. The reverse order of M_0 and M_1 is also admissible, but gives poorer results. Once M_α is known, the reflectance is

$$\mathscr{R}_\alpha^{\parallel,\perp}(\theta,\lambda) = 1 - \frac{4}{\|\mathsf{M}_\alpha\|^2 + 2}, \tag{18}$$

where $\|\mathsf{M}_\alpha\|^2 = \sum_{ij} |m_{ij}|^2$ (the sum of the absolute squares of the matrix elements) is the (Frobenius) norm of M_α.

Please, note carefully that this reflectance must be separately calculated for both basic polarizations. As usual, to avoid separate discussions for these two polarizations, we will work with the unpolarized reflectance

$$\mathscr{R}_\alpha(\theta,\lambda) = \frac{1}{2}[\mathscr{R}_\alpha^{\parallel}(\theta,\lambda) + \mathscr{R}_\alpha^{\perp}(\theta,\lambda)]. \tag{19}$$

As stressed by its explicit dependence, the expression for $\mathscr{R}_\alpha(\theta,\lambda)$ is valid for a fixed direction and wavelength. To deal with ODR, it seems convenient to average $\mathscr{R}_\alpha(\theta,\lambda)$ over the incidence angles (from 0 to $\pi/2$) and over the wavelengths in the spectral interval of interest $\Delta\lambda = \lambda_{\max} - \lambda_{\min}$. Accordingly, we introduce

$$\bar{\mathscr{R}}_\alpha = \frac{1}{\Delta\lambda} \int_{\lambda_{\min}}^{\lambda_{\max}} \left[\frac{2}{\pi} \int_0^{\pi/2} \mathscr{R}_\alpha(\theta,\lambda)\, d\theta \right] d\lambda. \tag{20}$$

When this wavelength- and angle-averaged reflectance satisfies $\bar{\mathscr{R}}_\alpha = 1$, we have broadband ODR. Yet this can be strictly accomplished only in the limit of infinite chains: in a finite system, one has to content oneself with $\bar{\mathscr{R}}_\alpha$ being close enough to unity, which we refer to as approximate broadband ODR.

The quantity $\bar{\mathscr{R}}_\alpha$ can be understood as a merit function respect to the unit ideal reflectance. In principle, more sophisticated merit functions are at hand [71–73], although the physical results do not depend of such a choice.

For given materials, $\bar{\mathscr{R}}_\alpha$ is a function of the layer thicknesses d_L and d_H. However, while the reflectance $\mathscr{R}_\alpha(\theta,\lambda)$ is a periodic function of d_L and d_H, this is not longer true for $\bar{\mathscr{R}}_\alpha$.

In what follows, we investigate the optimal thicknesses giving maximum $\bar{\mathscr{R}}_\alpha$. In all our computations the two thicknesses are varied independently from 0.02 μm to 0.30 μm. This

#198470 - $15.00 USD Received 1 Oct 2013; revised 14 Nov 2013; accepted 15 Nov 2013; published 27 Nov 2013

range is in turn subdivided into 50 even intervals, so all in all we get a set of 50×50 equal rectangles. The center of each rectangle is picked as an initial guess and we seek for the best point (i.e., the local optimum) by using a random permutation of the two thicknesses and an iterative search with fixed (positive or negative) increment.

In the next optimization step, we apply a quasiNewton algorithm (available in the NAG library) to improve the points of the previous exploration. Finally, the best of the 2500 local optima is taken as the global optimum thicknesses.

4. Narrowband ODR

For the time being, we analyze the narrowband approximation, in which the incident radiation can be regarded as monochromatic at wavelength λ. In such an instance, one can ignore the integration over the wavelength in (20) and the averaged reflectance reduces to

$$\bar{\mathscr{R}}_\alpha = \frac{2}{\pi}\int_0^{\pi/2} \mathscr{R}_\alpha(\theta,\lambda)\, d\theta. \tag{21}$$

Following the case study in [43] , we take the materials to be cryolite (Na_3AlF_6) and Zinc Selenide (ZnSe), with refractive indices $n_L = 1.34$ and $n_H = 2.568$, respectively, at $\lambda = 0.65\ \mu$m. This simple example allows one to work out easily the details of the method, which can be immediately extended to other media.

We have calculated the optimal thicknesses for several generations of the generalized Fibonacci sequences. All the information can be found in the datasets included in the Supplementary Material.

We recall that the usual ODR Bragg solution [39] consists of alternating quarter-wavelength layers (at normal incidence), namely

$$n_L d_L/\lambda = 1/4, \qquad n_H d_H/\lambda = 1/4, \tag{22}$$

which corresponds to physical thicknesses $d_L = 0.1213\ \mu$m and $d_H = 0.0633\ \mu$m. We cling to the practice of expressing the thicknesses in an adimensional form. For almost all the situations (except nickel and copper means), $n_L d_L/\lambda \simeq 0.28$. The optimal H thicknesses considerably vary from system to system. We thus end up that the quarter-wavelength solution (22) is not the optimal for ODR, as already noticed in [37].

In Fig. 3 we have represented $-\ln(1-\bar{\mathscr{R}}_\alpha)$ (calculated at the optimal thicknesses) as a function of the number of layers N_α. For all the generalized Fibonacci sequences, this magnitude increases linearly with N_α. As a matter of fact, we have applied the fitting

$$-\ln(1-\bar{\mathscr{R}}_\alpha) = a_0 + a_1 N_\alpha\,. \tag{23}$$

Table 1. Fitting parameters of the narrowband model (23) and the broadband model (25). In both cases, we include the Pearson correlation coefficients.

System	Metal	a_0	a_1	R^2	b_0	b_1	b_2	R^2
Periodic	—	1.249	0.279	0.999	0.450	2.675	0.253	0.931
FS(1,1)	Gold	2.186	0.112	0.991	0.831	2.086	0.046	0.939
FS(2,1)	Silver	1.469	0.134	0.997	0.811	2.790	0.030	0.937
FS(3,1)	Bronze	1.374	0.095	0.978	0.792	2.890	0.019	0.989
FS(1,2)	Copper	0.770	0.130	0.997	0.132	2.339	0.087	0.967
FS(1,3)	Nickel	1.715	0.035	0.953	0.799	4.123	0.010	0.961

#198470 - $15.00 USD Received 1 Oct 2013; revised 14 Nov 2013; accepted 15 Nov 2013; published 27 Nov 2013

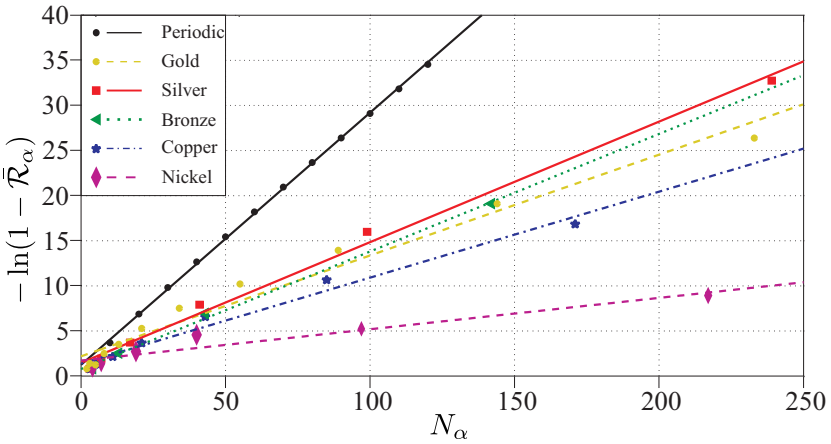

Fig. 3. Logarithm (with changed sign) of $1-\bar{\mathcal{R}}_\alpha$ [$\bar{\mathcal{R}}_\alpha$ is the angle-averaged reflectance (21)] for the optimal thicknesses and several generations of different generalized Fibonacci sequences as a function of the number of layers N_α.

The linear dependence is clearly observed for the periodic case, whereas for the other examples (especially, the nickel), the cloud of points is not large enough to appraise at a glance the goodness of the fit. Nonetheless, the correlation coefficients in Table 1 (which have been validated by enlarging the range of N_α) confirm that (23) is indeed a good approximation. Note, in passing, that this implies that $\bar{\mathcal{R}}_\alpha$ approaches the unity exponentially with N_α, as one would expect from an omnidirectional bandgap [39].

The periodic stack has the biggest slope, followed by the Olympic-metal family (taken in the order silver, bronze, and gold). Finally, the non-Olympic family performs the worst (copper and nickel). To sum up, as narrowband ODR is concerned, periodicity always beats both quasiperiodic and aperiodic orders.

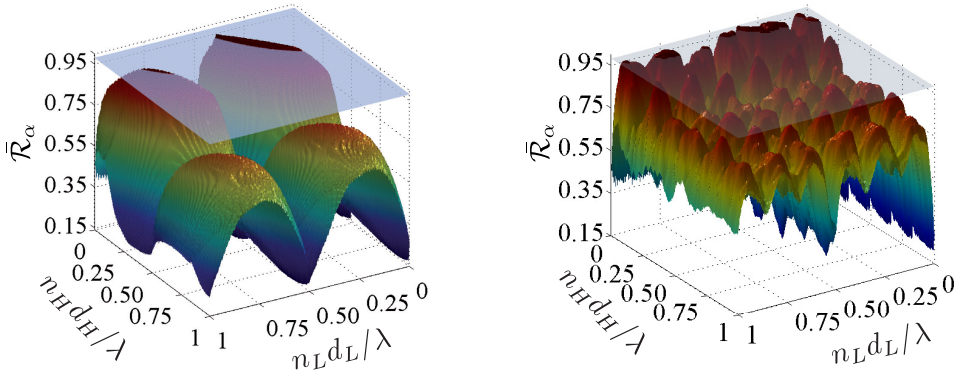

Fig. 4. Averaged reflectance $\bar{\mathcal{R}}_\alpha$ as a function of the adimensional thicknesses $n_L d_L/\lambda$ and $n_H d_H/\lambda$ (at a working wavelength of 0.65 μm) for the periodic system with 218 layers (left panel) and the nickel-mean system with 217 layers (right panel). In both figures, we include a plane of constant reflectance 0.98.

#198470 - $15.00 USD Received 1 Oct 2013; revised 14 Nov 2013; accepted 15 Nov 2013; published 27 Nov 2013

The long-range order of these arrangements is responsible for the anomalous interference giving rise to pseudo-bandgaps wherein $\bar{\mathscr{R}}_\alpha$ is close to unity. That order is reflected in the position and strength of the Bragg peaks in the Fourier spectrum, as illustrated in Fig. 2. In this respect, the photonic crystals present the sharpest localized peaks.

To gain further insights into these features, in Fig. 4 we have depicted the averaged reflectance $\bar{\mathscr{R}}_\alpha$ for the two most extreme situations according to the performance in the Fig. 3; periodic (with 218 layers) and nickel mean (with 217 layers), in terms of the adimensional thicknesses $n_L d_L/\lambda$ and $n_H d_H/\lambda$. We have also included a plane of constant reflectance 0.98, so that the regions above this plane determine the parameters in which approximate ODR happens.

For the periodic stack, $\bar{\mathscr{R}}_\alpha$ exhibits four fairly smooth humps, the highest centered around $n_L d_L/\lambda \simeq 0.30$ and $n_H d_H/\lambda \simeq 0.28$: the quarter-wavelength solution is accurate enough in this example. In contradistinction, the nickel-mean shows quite an oscillatory behavior, with slightly smaller peaks.

To round out the analysis, in Fig. 5 we have outlined the isocontours of $\bar{\mathscr{R}}_\alpha = 0.98$ for the generalized Fibonacci quasicrystals and generations picked out in such a way that all of them have a comparable number of layers. The filled regions represent again the range of adimensional thicknesses for which approximate ODR holds (we have restricted the values of these variables to the most interesting zone up to 0.5, i.e., half-wavelength thickness). We caution that the centers of these isles do not necessarily coincide with the optimal values listed in the Supplementary Material.

Several remarkable facts can be observed in this figure. First of all, for the periodic and the Olympic-metal family, these sectors are close to ellipses with the major axes orientated predominantly along the vertical axis (except the silver mean). For the non-Olympic metal family they are of irregular shape. The shaky contours are due to the strong oscillations already apparent in Fig. 4. As a second comment, the centers of the ellipses are distributed along either $n_H d_H/\lambda \simeq 0.28$ or $n_H d_H/\lambda \simeq 0.12$. The coordinates in the $n_L d_L/\lambda$ axis are, however, pretty diverse.

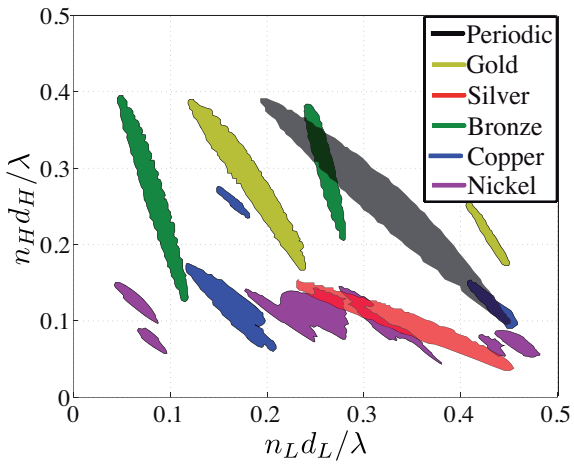

Fig. 5. Contours of $\bar{\mathscr{R}}_\alpha = 0.98$, as a function of the adimensional thicknesses $n_L d_L/\lambda$ and $n_H d_H/\lambda$ for the systems: periodic (218 layers), Olympic-metal family [gold (233 layers), silver (239 layers), bronze (142 layers)], and non-Olympic-metal family [copper (171 layers) and nickel (217 layers)].

#198470 - $15.00 USD Received 1 Oct 2013; revised 14 Nov 2013; accepted 15 Nov 2013; published 27 Nov 2013

These regions also delimit the thickness tolerances: the greater their extent, the better the tolerance. Consequently, the periodic crystal is clearly the best (the nickel sequence presents also a broad area, but split in many small islets). Furthermore, the orientation of these domains indicates that the tolerance in the H thickness is always bigger than in the L material (except for the silver mean, again).

5. Broadband ODR

We go farther along in our program and consider the incident radiation to have a spectral width $\Delta\lambda$, which extends from $\lambda_{\min} = 0.5\ \mu$m to $\lambda_{\max} = 0.8\ \mu$m. In this range, the refractive index of the cryolite can be considered, to a good approximation, as constant ($n_L = 1.34$), while for the Zinc Selenide we use the Sellmeier-type dispersion equation [74]

$$n_H^2(\lambda) = 4 + \frac{1.9\lambda^2}{\lambda^2 - (0.336)^2}\,, \tag{24}$$

with λ expressed in microns. This implies a smooth variation between $n_H(\lambda_{\min})$= 2.732 and $n_H(\lambda_{\max}) = 2.511$.

The quantity of interest is now the wavelength- and angle-averaged reflectance (20). As one can find out in the Supplementary Material, for the periodic and the Olympic-metal family, the optimal values of $n_L d_L/\lambda$ are close to 1/4, while for the H layers, this quarter-wavelength solution holds only for the periodic and the golden and nickel means.

In Fig. 6 we have plotted $-\ln(1-\bar{\mathscr{R}}_\alpha)$ for the same examples as in Fig. 3, as a function of the number of layers N_α, employing the optimal thicknesses. In this instance, the points can be appropriately fitted to the function

$$-\ln(1-\bar{\mathscr{R}}_\alpha) = b_0 + b_1[1-\exp(-b_2 N_\alpha)]\,. \tag{25}$$

The values of b_0, b_1, and b_2, as well as the correlation coefficients, are given in Table 1.

For small N_α (that is, $N_\alpha \ll b_2^{-1}$, so the concrete limit value depends on the sequence), this can be approximated by the straight line $-\ln(1-\bar{\mathscr{R}}_\alpha) \simeq b_0 + b_1 b_2 N_\alpha$, which is tantamount to an exponential increasing of $\bar{\mathscr{R}}_\alpha$. In this regime, again the photonic crystal is unbeatable.

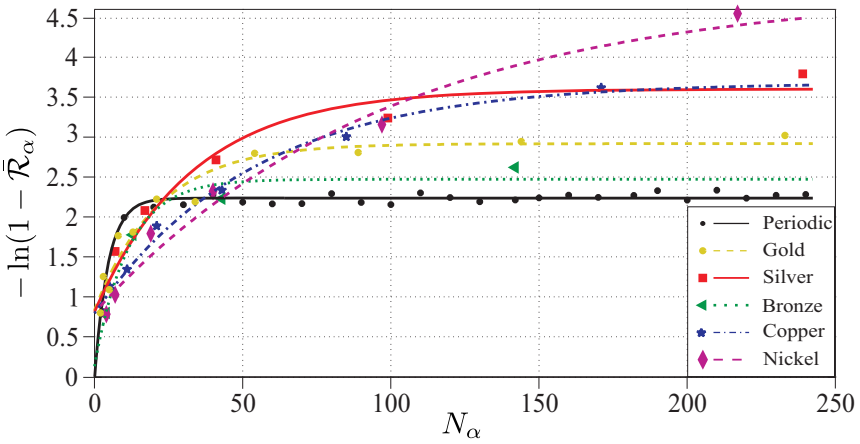

Fig. 6. Logarithm (with changed sign) of the $1-\bar{\mathscr{R}}_\alpha$ [$\bar{\mathscr{R}}_\alpha$ is the wavelength- and angle-averaged reflectance (20)] for the optimal thicknesses and the same generations of different generalized Fibonacci sequences as in Fig. 3, as a function of the number of layers.

#198470 - $15.00 USD Received 1 Oct 2013; revised 14 Nov 2013; accepted 15 Nov 2013; published 27 Nov 2013

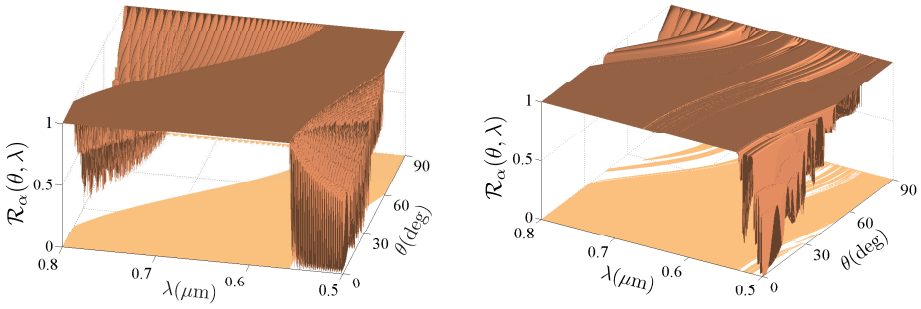

Fig. 7. Reflectance $\mathscr{R}_\alpha(\theta,\lambda)$ for the periodic (left panel, 218 layers) and the nickel-mean (right panel, 217 layers) sequences, as a function of the wavelength λ (in μm) and the incidence angle θ (in degrees). We have used the optimal thicknesses (in μm) ($d_L = 0.1391, d_H = 0.0568$) for the periodic and ($d_L = 0.0446, d_H = 0.0604$) for the nickel sequences.

However, in the opposite limit of large N_α ($N_\alpha \gg b_2^{-1}$), we have $-\ln(1-\bar{\mathscr{R}}_\alpha) \simeq b_0 + b_1$ and $\bar{\mathscr{R}}_\alpha$ saturates to a constant value, regardless of the number of layers. Now, the nickel family is by far the best choice, an unexpected result from all accounts. Indeed, it is the worst in the narrowband limit: another demonstration of how inescrutable are the ways of interference. In the transition between these two circumstances (which extends from around 30 to 100 layers), the silver mean offers the best achievements.

In Fig. 7 we show $\mathscr{R}_\alpha(\theta,\lambda)$ as a function of the wavelength and the incidence angle for the same arrangements as in Fig. 4. The filled contour at the bottom plane indicates the range of λ and θ for which $\mathscr{R}_\alpha(\theta,\lambda)$ is greater than 0.99. The periodic system exhibits a flat and smooth plateau of unit reflectance that quickly falls down with deep oscillations. On the contrary, for the nickel system the plateau is not so clean, due to the presence of wrinkles, but it is more outspread. This compromise is what makes the nickel sequence superior for broadband ODR.

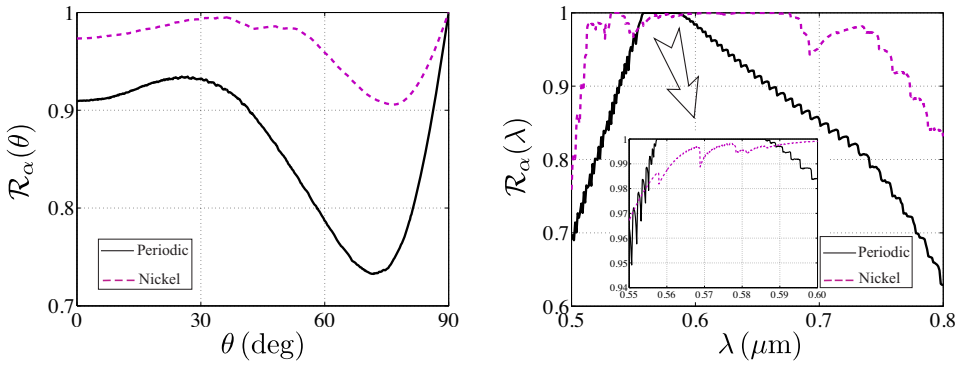

Fig. 8. Wavelength-averaged reflectance $\mathscr{R}_\alpha(\theta)$ versus the angle of incidence (left panel) and angle-averaged reflectance $\mathscr{R}_\alpha(\lambda)$ versus the wavelength (right panel), for the same examples as in Fig. 7. Black continuous line for the periodic system and purple broken line for the nickel sequence. For clarity, we have included an inset of the region where $\mathscr{R}_\alpha(\lambda)$ is greater for the periodic structure.

#198470 - $15.00 USD Received 1 Oct 2013; revised 14 Nov 2013; accepted 15 Nov 2013; published 27 Nov 2013

We can also look at this issue from an alternative viewpoint. Let us consider the functions

$$\mathscr{R}_\alpha(\theta) = \frac{1}{\Delta\lambda}\int_{\lambda_{\min}}^{\lambda_{\max}} \mathscr{R}_\alpha(\theta,\lambda)d\lambda\,, \qquad \mathscr{R}_\alpha(\lambda) = \frac{2}{\pi}\int_0^{\pi/2} \mathscr{R}_\alpha(\theta,\lambda)\,d\theta\,, \tag{26}$$

which correspond to partial averages over wavelength and angles, respectively, of the reflectance $\mathscr{R}_\alpha(\theta,\lambda)$. These quantities are plotted in Fig. 8 for the same samples as in Fig. 7. Obviously, the area under these curves is precisely $\bar{\mathscr{R}}_\alpha$. The function $\mathscr{R}_\alpha(\theta)$ is always worse for the periodic system, mainly because the deep and oscillating valleys noticeable in Fig. 7 make a poor contribution. On the other hand, $\mathscr{R}_\alpha(\lambda)$ is unity for the periodic system in a narrow range (from 0.56 μm to 0.59 μm), but falls quickly. For the nickel sequence, the wings of this curve are broader, giving then a bigger value of the integral.

This discussion indicates that approximate ODR may be attained either by getting $\mathscr{R}_\alpha(\lambda)$ somewhat close to unity across the entire range $\Delta\lambda$ or getting $\mathscr{R}_\alpha(\lambda)$ almost unity somewhere in that range, and significantly different from unity elsewhere (and then the setup acts as an efficient passband filter). Therefore, despite the fact that $\bar{\mathscr{R}}_\alpha$ is a practically valid metric, one needs to complement it with additional information. A good way of doing that is through the notion of omnidirectional bandwidth, which we adapt from the case of perfect ODR (where the bandgaps are well defined): if we denote by λ_+ and λ_- the longer- and shorter-wavelength edges for which $\mathscr{R}_\alpha(\lambda)$ drops to 0.707 (this is just a drop of 3 dB relative to the unity), it seems sensible to define [75]

$$B = \frac{\lambda_+ - \lambda_-}{\frac{1}{2}(\lambda_+ + \lambda_-)}\,. \tag{27}$$

This fractional ODR bandwidth is $B = 0.368$ for the periodic and $B = 0.461$ for the nickel mean in Fig. 8.

Another related point is the selection of the interval $\Delta\lambda$ entering the definition of $\bar{\mathscr{R}}_\alpha$. It is apparent from Fig. 8 that, for a different $\Delta\lambda$, one may reasonably expect significant differences, especially if $\Delta\lambda$ matches the bandgap of a particular sample. In fact, the bandgap of a periodic structure is simply narrower (and consequently, of better quality [76, 77]) than the pseudo-bandgap of generalized Fibonacci structures, and this causes the broadband ODR performance studied here. We have checked that with other choices of $\Delta\lambda$ the ranking in Fig. 6 changes.

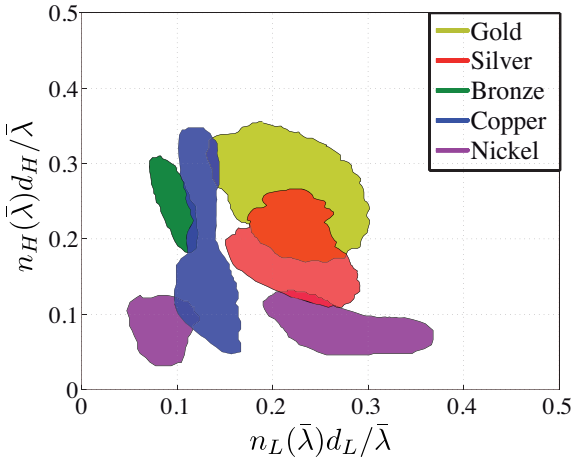

Fig. 9. Contour plots of $\bar{\mathscr{R}}_\alpha = 0.90$ in the broadband case, for the same arrangements as in Fig. 5.

#198470 - $15.00 USD Received 1 Oct 2013; revised 14 Nov 2013; accepted 15 Nov 2013; published 27 Nov 2013

Finally, to parallel as much as possible the treatment for narrowband ODR, in Fig. 9 we sketch the isocontours of $\bar{\mathscr{R}}_\alpha = 0.90$ for the same systems as in Fig. 5. To unify the presentation, we use the normalized thicknesses $n_L(\lambda)d_L/\lambda$ and $n_H(\lambda)d_H/\lambda$, where λ is the average wavelength, that coincides with 0.65 μm. Surprisingly enough, the periodic system performs so poorly that it does not appear. The ODR regions are now more irregular than in the narrowband limit.

6. Concluding remarks

To summarize, we have exploited the notion of wavelength- and angle-averaged reflectance to explore in a systematic way the performance of generalized Fibonacci sequences as ODRs. Our approach is general and can be applied to other materials and other spectral ranges. What we have discovered is that, quite unexpectedly, these sequences can perform much better than the photonic crystals, while providing more versatility. We think that this constitutes a unique fact that might open avenues for quasicrystals.

Acknowledgments

Financial support from the Spanish DGI (Grant FIS2011-26786) is gratefully acknowledged.

#198470 - $15.00 USD Received 1 Oct 2013; revised 14 Nov 2013; accepted 15 Nov 2013; published 27 Nov 2013